Three-Dimensional Solution Structure of Lactoferricin B, an Antimicrobial Peptide Derived from Bovine Lactoferrin†

Peter M. Hwang,‡ Ning Zhou,‡ Xi Shan,§ Cheryl H. Arrowsmith,§ and Hans J. Vogel*,‡

Department of Biological Sciences, University of Calgary, Calgary, Alberta T2N 1N4, Canada, and Division of Molecular and Structural Biology, Ontario Cancer Institute, University of Toronto, Toronto, Ontario M5G 2M9, Canada

Received September 17, 1997; Revised Manuscript Received December 23, 1997

ABSTRACT: The solution structure of bovine lactoferricin (LfcinB) has been determined using 2D ^{1}H NMR spectroscopy. LfcinB is a 25-residue antimicrobial peptide released by pepsin cleavage of lactoferrin, an 80 kDa iron-binding glycoprotein with many immunologically important functions. The NMR structure of LfcinB reveals a somewhat distorted antiparallel β-sheet. This contrasts with the X-ray structure of bovine lactoferrin, in which residues 1−13 (of LfcinB) form an α-helix. Hence, this region of lactoferricin B appears able to adopt a helical or sheetlike conformation, similar to what has been proposed for the amyloidogenic prion proteins and Alzheimer's β-peptides. LfcinB has an extended hydrophobic surface comprised of residues Phe1, Cys3, Trp6, Trp8, Pro16, Ile18, and Cys20. The side chains of these residues are well-defined in the NMR structure. Many hydrophilic and positively charged residues surround the hydrophobic surface, giving LfcinB an amphipathic character. LfcinB bears numerous similarities to a vast number of cationic peptides which exert their antimicrobial activities through membrane disruption. The structures of many of these peptides have been well characterized, and models of their membrane-permeabilizing mechanisms have been proposed. The NMR solution structure of LfcinB may be more relevant to membrane interaction than that suggested by the X-ray structure of intact lactoferrin. Based on the solution structure, it is now possible to propose potential mechanisms for the antimicrobial action of LfcinB.

Lactoferrin is an 80 kDa iron-binding glycoprotein present in milk and other exocrine secretions (*1*). It is also found in the granules of polymorphonuclear leukocytes (*2*) and is released during inflammatory responses (*3*). Lactoferrin provides a natural defense against a wide range of bacteria (*4*, *5*) and fungi (*6*, *7*). Originally, the antimicrobial activity of lactoferrin was attributed entirely to its iron-sequestering capabilities. However, a peptide fragment near the N-terminus of lactoferrin was recently found to have a more potent bactericidal effect than intact lactoferrin itself (*8*). The peptide, named lactoferricin (Lfcin),[1] has a lethal effect on a wide range of microorganisms (*9*, *10*).

Bovine lactoferricin (LfcinB) has a higher bactericidal potency than human lactoferricin (LfcinH) (*8*). LfcinB is a 25-amino acid peptide with the sequence ^{17}FKCRR WQWRM KKLGA PSITC VRRAF. The two cysteines are linked by a disulfide bridge which is also present in intact lactoferrin, but this is not essential for bactericidal activity (*8*). Although the antimicrobial effects of Lfcin have been well characterized, its mechanism of action is currently poorly understood. The primary sequence of LfcinB contains many hydrophobic and positively charged residues, suggesting that it may interact with biological membranes. Indeed, membrane blisters have been observed in bacteria exposed to Lfcin (*11*), and it binds to lipopolysaccharide, the major component of the outer leaflet of Gram-negative bacterial outer membranes (*12*, *13*).

LfcinH and LfcinB are released by proteolytic cleavage of intact human or bovine lactoferrin by pepsin. Lfcin may therefore play an antimicrobial role within the infant gastrointestinal tract (*14*). It is also suspected to play a broader role in host defense—lactoferrin has a number of other immunologically important functions (*15*) besides its antimicrobial activity. Lactoferrin limits inflammation by inhibiting production of tumor necrosis factor α, interleukin-1 (*16*), and interleukin-6 (*17*). These functions may be related to lipopolysaccharide binding by lactoferricin, since LPS stimulates production of these factors. In addition, lactoferrin has been implicated in the stimulation of many immunologi-

† Supported by operating grants from the Medical Research Council of Canada to C.H.A. and H.J.V. P.M.H. and H.J.V. hold a Studentship and Scientist Award from the Alberta Heritage Foundation for Medical Research.

* To whom correspondence should be addressed. Telephone: 403-239-1138. Fax: 403-289-9311. Email: vogel@acs.ucalgary.ca.

‡ University of Calgary.

§ University of Toronto.

[1] Abbreviations: LfcinB, bovine lactoferricin; LfcinH, human lactoferricin; 2D, two-dimensional; NMR, nuclear magnetic resonance; HPLC, high-performance liquid chromatography; UV, ultraviolet; FTIR, Fourier transform infrared; DQF-COSY, double-quantum-filtered 2D correlation spectroscopy; TOCSY, 2D total correlation spectroscopy; NOE, nuclear Overhauser effect; NOESY, 2D NOE spectroscopy; WATERGATE, water suppression by gradient-tailored excitation; DSS, 4,4-dimethyl-4-silapentane-1-sulfonate; RMSD, root-mean-square deviation; LPS, lipopolysaccharide.

S0006-2960(97)02323-4 CCC: $15.00
Published on Web 03/03/1998

cal cells, including natural killer cells, lymphokine-activated killer cells (*18*), polymorphonuclear leukocytes, and macrophages (*19*). The activation of natural killer cells and other immune components may be related to the recently discovered tumor growth suppression exhibited by lactoferrin (*20*). LfcinB has also been found to inhibit tumor growth, but whether this is more related to its antimicrobial activity or to any stimulatory effect on the immune system has yet to be established (*21*).

Lfcin is one of a vast array of cationic antimicrobial peptides (*22*, *23*). It bears similarities to several major classes of these peptides. Some, like the cecropins (*24*) and magainins (*25*), form amphipathic helices upon binding to membranes (*26*, *27*). Lfcin does bear some homology to the magainins and may be able to form an amphipathic helix (*28*). Another major class of antimicrobial peptides includes the defensins (*29*) and β-defensins (*30*), which contain three disulfide bridges and form three antiparallel β-strands (*31*, *32*). Protegrins (*33*) and tachyplesins (*34*) contain two disulfide bridges and two antiparallel β-strands; Lfcin contains a single disulfide bridge, and could potentially form a similar β-sheet. Finally, the two Trp residues in LfcinB may suggest a similar mode of action to the tryptophan-rich antibacterial peptides, indolicidin (*35*) and tritrpticin (*36*). The mode of action for all antimicrobial cationic peptides is still much debated, and the exact mechanism for Lfcin may contain aspects similar to more than one of the cationic antimicrobial peptide classes.

The structure of bovine lactoferrin has recently been solved by X-ray diffraction (*37*). It closely resembles the structure of human lactoferrin (*38*, *39*). In intact bovine lactoferrin, the region corresponding to LfcinB is partially solvent-exposed, where it could potentially interact with cell membrane components such as lipopolysaccharide or cellular receptors. In this study, the solution structure of lactoferricin B has been solved by conventional 2D NMR methods. The secondary structure of the antimicrobial peptide is different from that observed in the crystal structure of intact bovine lactoferrin. This different conformation may be relevant to the increased bactericidal activity of LfcinB compared to intact bovine lactoferrin.

EXPERIMENTAL PROCEDURES

Sample Preparation. Lactoferricin B was synthesized at the Peptide Synthesis Facility at Queen's University and HPLC-purified by Dr. Dennis McMaster at the University of Calgary. The two cysteines were oxidized to form an intramolecular disulfide bridge. The peptide purity and composition were confirmed by mass spectrometry. A 3 mM lactoferricin B NMR sample was produced by dissolving lyophilized LfcinB powder in 90% H_2O/10% D_2O. The concentration was determined by UV absorbance and a theoretically determined $\epsilon(280)$ of 11 125 M^{-1} cm^{-1} (*40*). The pH was adjusted to 4.5 using minute amounts of HCl and KOH. D_2O samples were lyophilized and redissolved in 99.99% D_2O. This process was repeated twice. The chemical shift reference compound DSS was added to all samples.

Fluorimetry and Mass Spectrometry. Fluorescence spectra were obtained with a Hitachi F-2000 fluorescence spectrophotometer. Samples of 5, 20, 80, and 200 μM LfcinB in 5 mM citrate, pH 4.5, were prepared for fluorescence measurements. A solution containing only 5 mM citrate, pH 4.5, was used as a blank. All samples were excited at a wavelength of 295 nm, and the emission spectra were recorded from 300 to 450 nm.

Electrospray mass spectrometry was performed on a Micromass Quattro II triple-quadrupole mass spectrometer operating in the negative ion mode. The temperature of the electrospray source was maintained at 55 °C. The buffer used was 4.5 mM NH_4HCO_3 (pH 8.0).

NMR Spectroscopy. Most ^{1}H NMR spectra were obtained on a Bruker AMX500 spectrometer. The spectra were processed using the standard UXNMR software on a Bruker X32 data station. All spectra were base-line-corrected and zero-filled to 1K in the F1 dimension. The F2 dimension contained 2K real points. DQF-COSY (*41*), TOCSY (*42*), and NOESY (*43*) spectra were recorded at 25 °C and in 90% H_2O/10%D_2O and used to obtain chemical shift assignments. The water signal was suppressed by low-power irradiation. Several NOESY spectra were acquired in an attempt to assign ambiguous peaks and clarify structural constraints. Two 200 ms mixing time NOESY spectra were obtained using solvent presaturation, one at 17 °C and the other at 25 °C. Another NOESY spectrum was recorded in D_2O with a 250 ms mixing time. Finally, one NOESY spectrum with 150 ms mixing time was run on a Varian Unity Plus 500 MHz spectrometer using WATERGATE (*44*) solvent suppression. The latter was processed with NMRPIPE (*45*) and viewed with NMRVIEW3 (*46*).

Structure Calculations. $^3J_{N\alpha}$ coupling constants were obtained from the DQF-COSY. If $^3J_{N\alpha}$ for a given residue was well resolved and greater than 9 Hz, the ϕ dihedral angle was constrained between $-80°$ and $-160°$. If $^3J_{N\alpha}$ was less than 5 Hz, ϕ was restricted between $-35°$ and $-85°$. For residues without well-resolved coupling constants and dihedral restraints, ϕ was constrained between $-35°$ and $-175°$, which includes all sterically permissible values for non-Gly residues. (The Gly14 ϕ angle was not restrained.) Structures without these dihedral restraints were also generated and showed that the extra restraints did not alter the peptide conformation significantly, although they did lower the backbone RMSD somewhat (see below). Many of the structures generated without the extra dihedral restraints had poor backbone stereochemistry.

Distance restraints were obtained from the NOESY spectra. Using an internal reference within the peptide, all NOE cross-peaks were classified as strong, medium, or weak. These were assigned upper limits of 2.7, 3.5, and 5.0 Å, respectively. The lower bounds were not specified, so the minimum distance between any two protons was limited by their van der Waals radii. Pseudoatom corrections were applied to the upper limits of degenerate or unassigned methylene, methyl, or phenylalanine ring groups (*47*). In addition, 0.5 Å was added to all short- and medium-range restraints involving methyl groups.

Structural calculations were performed with X-PLOR v. 3.851 using the simulated annealing protocol (*48*). A fully extended starting structure was generated. The disulfide bridge was broken and replaced by a regular NOE distance restraint between the two sulfur atoms. The starting structure was subjected to 18 000 steps of molecular dynamics at 1000 K, followed by 9000 cooling steps to 100 K. A 5 fs time

step was used. Finally, 200 steps of Powell energy minimization were performed. At all times, the structure was subject to dihedral restraints as well as the initial NOE distance restraints. Using this method, 100 structures were generated.

The structures were then examined to determine more precise structural information. Ambiguous NOESY cross-peaks were assigned, and stereospecific assignments were obtained where possible. In addition, potential hydrogen bonding pairs were identified. Hydrogen bonds were simulated by two distance restraints: a 3.3 Å restraint between the amide nitrogen and carbonyl oxygen and a 2.3 Å restraint between the amide hydrogen and carbonyl oxygen. The new structural information was applied in the simulated annealing refinement, which employed a softening of the van der Waals repulsions. All 100 structures were passed through the refinement, which consisted of 12 000 cooling steps from 1000 K followed by 5000 steps of Powell energy minimization. The disulfide bond remained intact during this calculation. Finally, structures with NOE restraint violations greater than 0.3 Å were discarded, and the 20 structures with the lowest energy were selected.

The same protocol for generation of structures was repeated without the use of the extra coupling constants (not based on the DQF-COSY) or hydrogen bonding constraints to ensure that these did not excessively influence the structure calculations.

RESULTS

LfcinB Has a Monomeric Structure. 1D ^{1}H NMR spectra of LfcinB at 1.5 and 0.15 mM indicated the absence of any concentration-dependent changes in the amide chemical shifts or peak line widths. Moreover, no NOE cross-peaks indicative of dimeric or multimeric structure were detected. Fluorescence measurements indicated that both tryptophans in LfcinB fluoresced at 350 nm over a concentration range from 5 to 200 μM. This emission wavelength is typical for solvent-exposed tryptophans, suggesting that LfcinB exists as a monomer in solution. In addition, electrospray mass spectrometry, performed under conditions where protein−peptide and peptide−peptide interactions are detected, showed lactoferrin B to run as a monomer. The observation that LfcinB is a monomer in solution is consistent with the high abundance of positively charged residues and the total absence of negatively charged residues. Similar results have been reported for other amphiphilic antimicrobial peptides.

Sequential Assignment. The proton resonances were identified using the methods proposed by Wüthrich (*49*). The final chemical shift assignments are shown in Table 1. A near-complete assignment of the proton resonances was obtained. The methyl group of Met10 was never observed, and the entire lengths of the Lys2 and Lys11 side chains could not be unambiguously assigned. The 3,5 ring protons of Phe25 and the ring proton at positions 4 of Phe1 and Phe25 were either not observed or not resolved.

Spin systems were identified using the TOCSY spectrum. The fingerprint region of the TOCSY spectrum is shown in Figure 1. The DQF-COSY spectrum was important for the complete characterization of the spin systems, and was particularly important for identifying the protons of the Trp indole groups and aliphatic side chains. The high degree of overlap near the diagonal between 1.3 and 1.8 ppm due to the 5 Arg and 3 Lys residues made this region uninterpretable in the two-dimensional DQF-COSY. Hence, the assignments of βH, γH, and δH relied on peak intensities in the NOESY and TOCSY spectra and are thus not absolutely certain. The spin systems were correlated to specific residues by comparing the NOESY with the TOCSY. The amide−α region of the NOESY is shown in Figure 2.

Table 1: ^{1}H Chemical Shifts (ppm) for LfcinB at 25 °C, pH 4.5[a,b]

	NH	αH	βH	γH	other H
Phe1		4.34	3.20		2,6H: 7.35
					3,5H: 7.22
Lys2	8.68	4.43	1.71, 1.76		
Cys3	8.79	4.52	HB1: 2.82		
			HB2: 2.70		
Arg4	8.77	4.37	1.56	1.77	δH: 3.11
					εH: 7.18
Arg5	7.85	4.40	1.62, 1.68	1.45	δH: 3.11
					εH: 7.21
Trp6	8.67	5.01	3.06	1H: 10.10	2H: 7.12
				4H: 7.34	5H: 7.01
				6H: 7.20	7H: 7.46
Gln7	8.81	4.58	1.86, 1.98	2.20	NH_z: 6.90
					NH_e: 7.48
Trp8	8.63	4.87	3.21	1H: 10.17	2H: 7.24
				4H: 7.49	5H: 7.09
				6H: 7.21	7H: 7.44
Arg9	8.61	4.46	1.70, 1.81	1.50	δH: 3.14
					εH: 7.15
Met10	8.46	4.45	1.99, 2.08	2.56	
Lys11	8.42	4.36	1.70, 1.82	1.38	δH: 1.44
Lys12	8.30	4.21	1.80	1.41	δH: 1.71
					εH: 2.98
					ζH: 7.55
Leu13	8.19	4.33	1.68	1.61	δH: 0.91
Gly14	8.34	HA1: 4.06			
		HA2: 3.91			
Ala15	8.11	4.65	1.37		
Pro16		4.60	HB1: 2.25	2.00	HD1: 3.78
			HB2: 1.88		HD2: 3.64
Ser17	8.49	4.69	3.83		
Ile18	8.34	4.48	1.38	HG11: 1.05	δH: 0.42
				HG12: 0.77	
				CH_3: 0.62	
Thr19	8.56	4.68	4.07	1.16	
Cys20	8.90	4.49	HB1: 2.50		
			HB2: 3.04		
Val21	8.44	4.23	2.09	HG1: 0.89	
				HG2: 0.81	
Arg22	7.96	4.39	1.68	1.49, 1.57	δH: 3.09
					εH: 7.11
Arg23	8.55	4.35	1.63, 1.68	1.40, 1.46	δH: 2.92
					εH: 6.95
Ala24	8.28	4.28	1.29		
Phe25	7.67	4.38	HB1: 2.97		2,6H: 7.22
			HB2: 3.14		

[a] All chemical shifts reported are relative to DSS. [b] In the case of stereospecific assignments, the nomenclature used by X-PLOR is used.

Secondary Structure. A compilation of observed inter-residue NOE's is shown in Figure 3. The pattern of long-range NOE's strongly suggests that LfcinB has an antiparallel β-sheetlike conformation. The extended conformation was apparent from the strong sequential α_i−NH_{i+1} peaks observed in the NOESY (Figure 2). The intraresidue α_i−NH_i peaks were much weaker and sometimes not even detected. In addition, sequential NH_i−NH_{i+1} peaks were not observed, which is typical of an extended conformation. One exception was the turn region from Lys12 to Ala15, which contained strong intraresidue α_i-NH_i peaks, as well as NH_i-NH_{i+1} peaks.

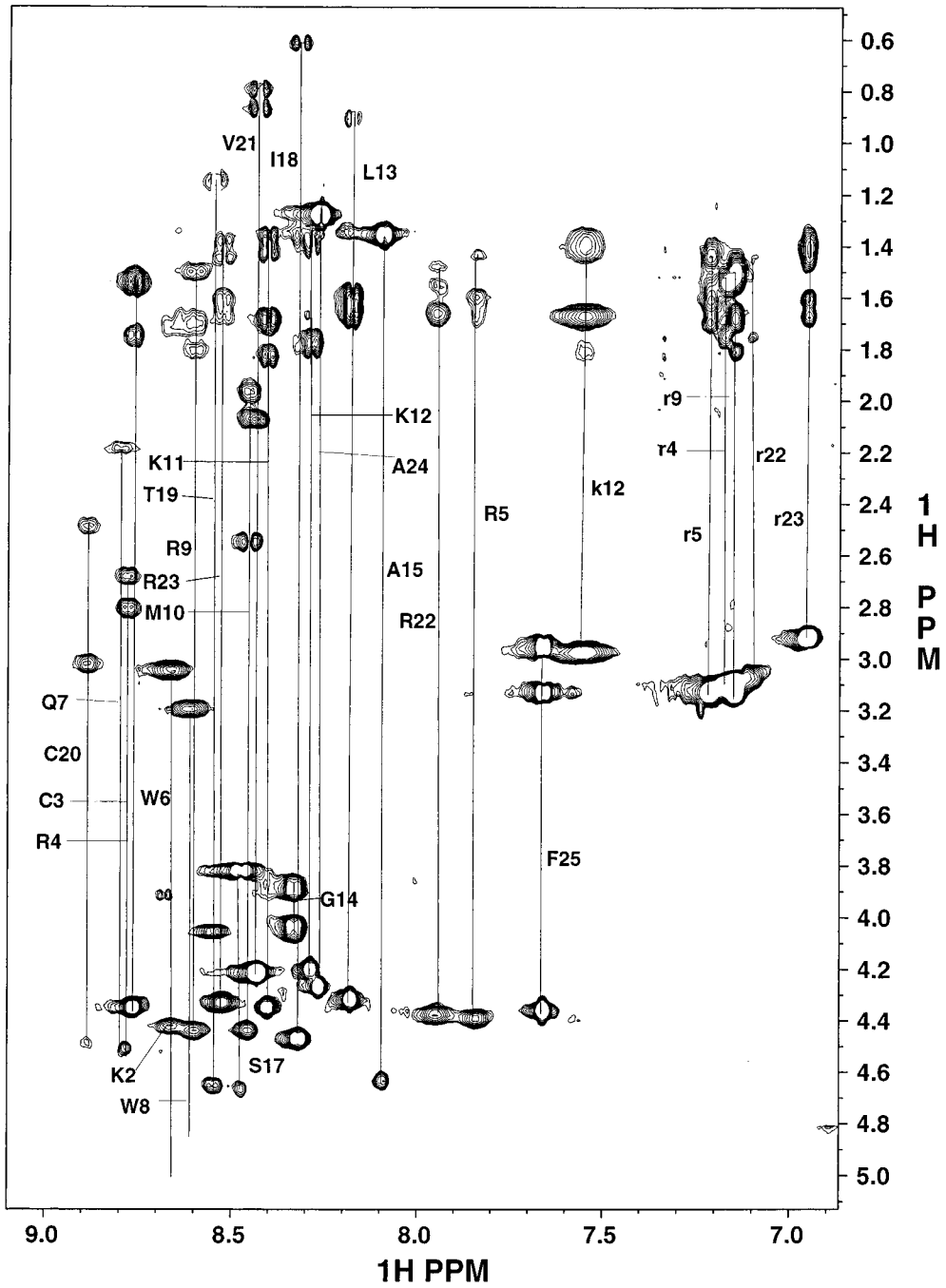

FIGURE 1: Fingerprint region of a TOCSY spectrum of LfcinB in 90% H_2O/10% D_2O at 25 °C, pH 4.5. The spin systems of the amide protons are designated by the amino acid one-letter code, upper case letters. The spin system of side chain nitrogen-bound protons is indicated with the amino acid one-letter code, lower case letters.

Many of the typical NOE's for β-sheets were observed across the strands, most notably between the α protons of Trp6 and Cys20, Trp8 and Ile18, and Met10 and Pro16. Unfortunately, many of the NOE's involving amides could not be observed, perhaps due to the relatively broad amide peaks. LfcinB contains only one proline residue, Pro16. The NOE patterns clearly indicated that Pro16 was in the trans configuration.

Strong sequential NH_i-NH_{i+1} peaks were also observed between Arg4 and Arg5 as well as Val21 and Arg22. These were indicative of two noticeable kinks in the extended structure near the disulfide bridge. The bend between Arg4 and Arg5 may be the result of the extended conformation accommodating the disulfide bond. The side chains of Cys3 and Trp6 would be expected to be on opposite sides of the backbone in a regular β-strand (they would be on the same side in an α-helix). However, Trp6 forms a hydrophobic surface which includes Ile18 and Cys20. Since Cys20 is connected to Cys3 by a disulfide bond, the side chain of Cys3 is forced to be on the same side as Trp6 (see Figure 4), introducing a noticeable kink between Cys3 and Trp6. This may induce a bend in the opposite strand between Cys20 and Arg22.

All of the initial structures generated with low NOE distance restraint violation showed that the amide hydrogens and carbonyl oxygens of Arg9 and Ser17 were suitably

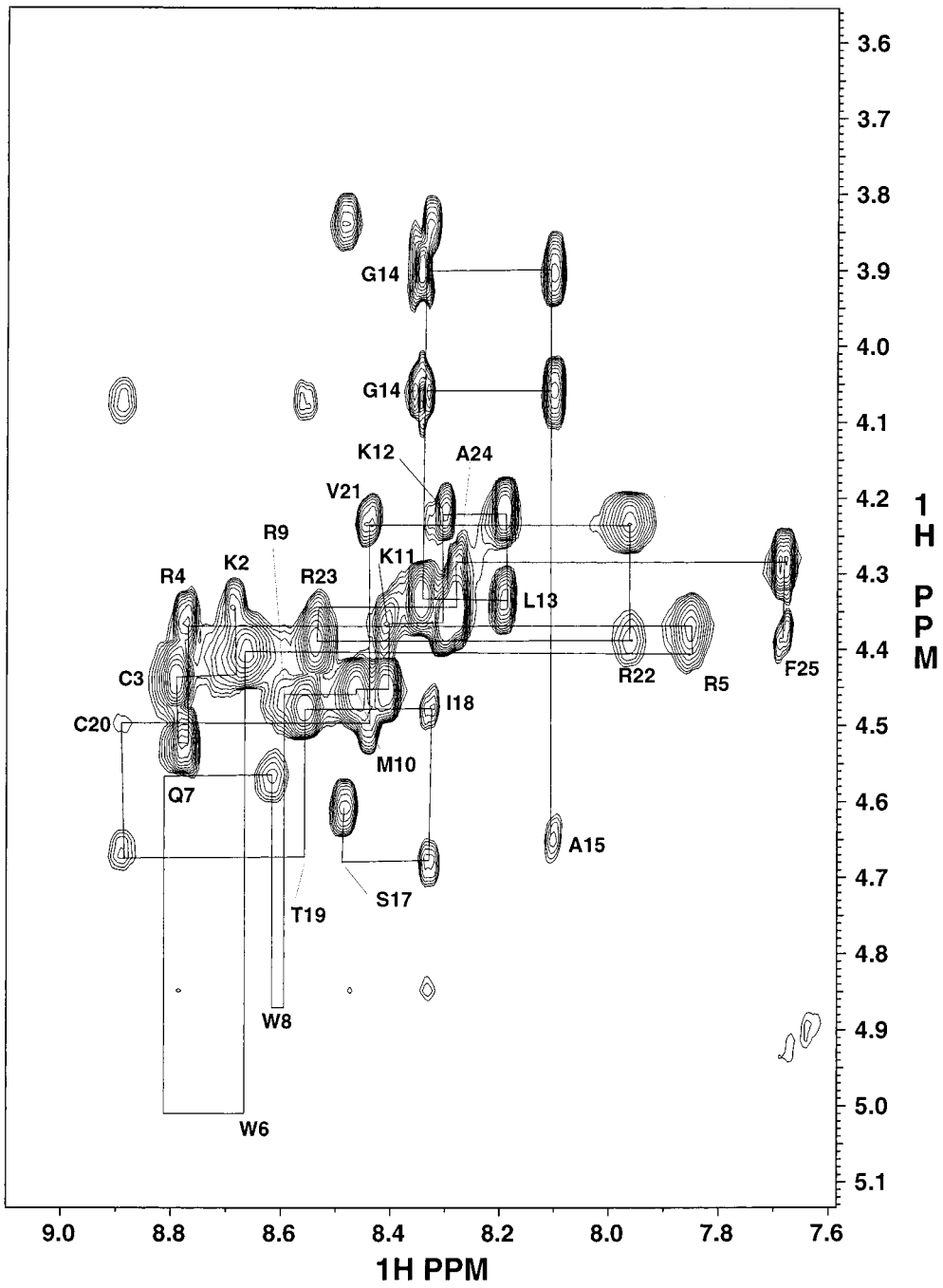

FIGURE 2: Amide−α region of a 200 ms mixing time NOESY spectrum of LfcinB in 90% H_2O/10% D_2O at 25 °C, pH 4.5. $H\alpha_i-NH_{i+1}$ connectivities are shown for residues 2−15 and 17−25. Residue 16 is a proline. For the sake of clarity, only the intraresidue α-amide peaks are labeled. In the cases where a peak is missing, a line is drawn to the position the peak would be expected, based on the chemical shift assignments obtained from other spectra.

oriented for hydrogen bonding. Hence, hydrogen bonds in the form of distance restraints between these atoms were introduced into the next round of calculations. Other potential hydrogen bonding pairs include Gln7−Thr19, and Lys12−Ala15. Deuterium exchange studies revealed that all amide protons were quickly exchanging with the solvent. Thus, the backbone may be somewhat flexible, allowing hydrogen bonds to transiently form and break. A comparison between the NOESY spectra taken at 17 and 25 °C revealed that the amide proton chemical shifts of Gln7, Arg9, Ala15, Ser17, and Thr19 were less sensitive to changes in temperature than other amide protons, which is typical for hydrogen-bonded protons.

Structure Calculations. After ineffective NOE restraints were removed, the initial structure calculations involved 237 NOE distance restraints. Final structure calculations involved 76 intraresidue, 84 sequential, 16 medium-range (less than i, i+5), and 91 long-range distance restraints. In total, 271 NOE restraints were used (including 4 hydrogen bonding restraints). From the DQF-COSY, seven residues were determined to have $^3J_{N\alpha}$ greater than 9.0 Hz. These residues were restrained to ϕ dihedral angles typical for extended conformations. All other residues were restrained to sterically allowed ϕ angles.

All of the final 20 structures generated well satisfied the NOE distance restraints, with no violations greater than 0.3

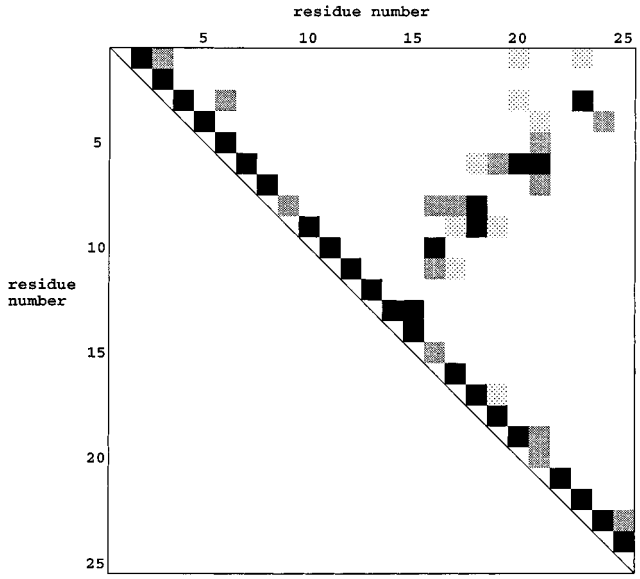

FIGURE 3: Summary of NOE's observed in LfcinB. A black square indicates a backbone−backbone NOE, a gray square indicates a backbone−side chain NOE, and a dotted square indicates a side chain−side chain NOE.

Å. The α carbons of the final 20 structures were superimposed on the mean structure and are shown on the left of Figure 5. There seem to be at least two major conformations possible at the turn region between residues 12 and 15. The two conformations may actually both occur, or perhaps the NOE data are insufficient to ascertain the correct conformation. To ensure that the extra dihedral restraints (not based on the DQF-COSY) and hydrogen bonding restraints did not result in a different global fold, 20 final structures were generated without them, and these are shown on the right of Figure 5. Indeed, the global conformation is similar. The only noticeable difference is that more conformations are available to the turn region.

When compared to the average structure, the mean RMSD for the 20 best structures was 0.64 Å for backbone atoms and 1.30 Å for all heavy atoms. (Without the extra dihedral restraints and hydrogen bond restraints, these values are 0.83 and 1.52 Å, respectively.) A RMSD per residue plot is shown in Figure 6. The backbone of the N- and C-terminal residues, 1−2 and 23−25, are poorly defined. Although there were NOE's observed between the ring protons of Phe1 and the methylene βH of Cys3 and Cys20, these were insufficient to resolve the interaction with the disulfide bridge or to fix the backbone. In addition, the backbone of the turn region between Lys12 and Ala15 is poorly defined. This may be due to some flexibility imparted to this region by Gly14, which, with the exception of Phe1, had the highest backbone RMSD. The charged side chains of Arg and Lys, as well as Gln7, had high RMSD values. The side chains of Met10 and Leu13 were also not well resolved. It is uncertain whether this is the result of conformational flexibility or a lack of distance restraints for these residues. Many of the hydrophobic side chains were well-defined, having RMSD's less than 0.5 Å.

Clustering of Hydrophobic Residues. Many of the hydrophobic residues of LfcinB are clustered on one side of the β-sheet. The side chains of Cys3, Trp6, Trp8, Pro16, Ile18, and Cys20 are well-defined, due to the many NOE cross-peaks observed between them. NOE's were detected showing Phe1 to be near the disulfide bridge, placing Trp6 between Ile18 and the disulfide bridge, and sandwiching Trp8 between Pro16 and Ile18. There were many NOE cross-peaks observed, indicating intimate interaction between these side chains. In addition, Leu13 and Ala15 of the turn region were positioned on the same side of the β-sheet as the other hydrophobic residues, even though no NOE's were observed with other hydrophobic residues. Thus, Phe1, Cys3, Trp6, Trp8, Leu13, Ala15, Pro16, Ile18, and Cys20 comprise a prominent hydrophobic surface shown in Figure 7. The high degree of hydrophobic interactions may be the principal driving factor for the folding of the LfcinB peptide. There was one hydrophilic residue which appeared on the hydrophobic side of LfcinB—this was Lys2 (see below), which did not have a well-defined position.

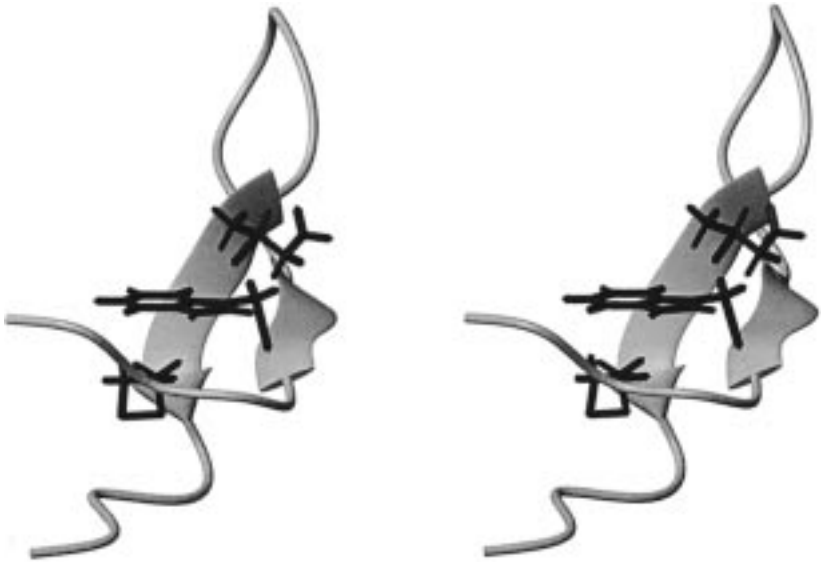

FIGURE 4: Stereoview of a ribbon diagram of LfcinB. The side chains of Ile18 and Cys20 are shown on the left strand, and the side chains of Trp6 and Cys3 are shown on the right strand. Cys3 and Cys20 form a disulfide bridge. The figure was generated using MOLMOL (Institut fuer Molekularbiologie und Biophysik, ETH Zurich Spectrospin AG, Faelanden, Switzerland).

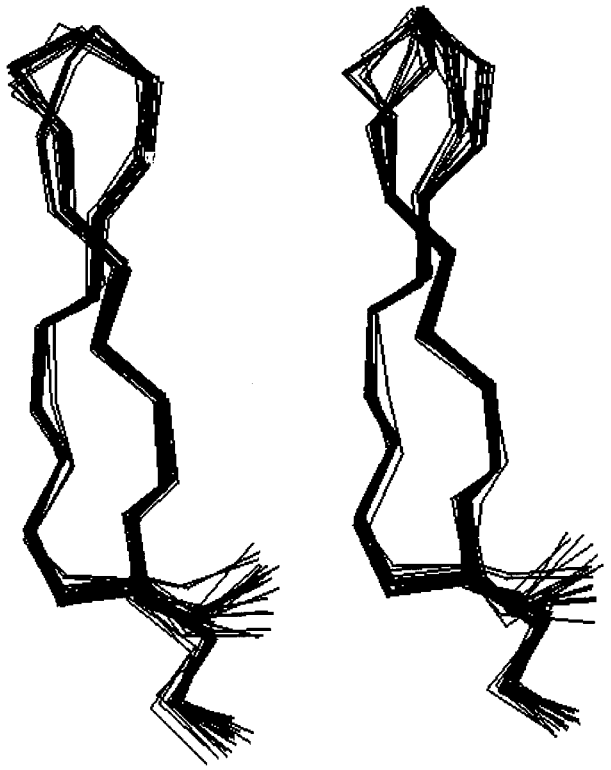

FIGURE 5: Left: 20 final structures of LfcinB superimposed on the mean structure. The RMSD for backbone atoms is 0.64 Å, and for heavy atoms, 1.30 Å. Right: 20 structures obtained without nonexperimental dihedral restraints and hydrogen bonding restraints, superimposed on the mean structure. The RMSD for backbone atoms is 0.83 Å, and for heavy atoms, 1.52 Å. Only the α carbons are shown. The figure was generated using INSIGHTII (Biosym, San Diego, CA).

Outside this hydrophobic strip, most side chains are hydrophilic or positively charged, including Arg4, Arg5, Gln7, Arg9, Lys11, Lys12, Ser17, Thr19, Arg22, and Arg23. These residues are shown in Figures 8 and 9. Figure 8 shows a mainly hydrophilic region which is on the opposite side of the hydrophobic strip, for which NOE's were observed between the side chains shown (refer to Figure 3). Figure 9 displays all the positively charged side chains of LfcinB. Looking down the β-strands toward the turn, Lys11-Lys12 are pointed to the left, and Arg4-Arg5 are oriented to the right. Above the backbone are located most of the hydrophobic residues (see Figure 7). Below the backbone are the rest of the hydrophilic residues, including Arg9, Arg22, and Arg23. Surprisingly, Met10 was located on the hydrophilic side. No long-range NOE's were observed for the Met10 side chain protons, which gave the side chain a high degree of flexibility in the structural models. A cross-strand $\alpha\alpha$ NOE was observed between Met10 and Pro16 which normally orients the side chains onto the same side for antiparallel β-sheets. However, the backbone begins to twist in order to accommodate the turn from Lys12 to Ala15. This pulls the Met10 side chain away from Pro16 and isolates it, perhaps explaining why no long-range NOE's involving the Met10 side chain were observed.

Another hydrophobic residue which appears on the hydrophilic side is Val21 (see Figure 8). Unlike Met10, the position of the Val21 side chain is well-defined, due to a large number of long-range NOE's between the methyl groups of Val21 and the methylenes of Arg5 and Gln7. Weaker and fewer interactions are observed between Val21 and Arg4 and Thr19. Even though Val21 exists on the hydrophilic side, its hydrophobic side chain is still somewhat shielded from solvent.

DISCUSSION

Interaction of Lactoferricin B with Membranes. The amphiphilicity observed in the lactoferricin B solution structure suggests that it is capable of interacting with biological membranes. Many of the hydrophobic residues are clustered to one side (see Figure 7), while the majority of the positively charged side chains are positioned outside this area, with the exception of Lys2 (see Figure 9). The hydrophobic residues could interact with the fatty acyl groups of the lipid bilayer while the positively charged Arg and Lys side chains interact with phosphodiester groups. Upon membrane binding, an even more efficient partitioning of hydrophobic and hydrophilic residues would be expected. Phe1, Lys2, Met10, Ala24, and Phe25 would all be able to adjust to the membrane environment, along with the long Lys and Arg side chains.

Elucidation of the bactericidal mechanism of lactoferricin will require an understanding of how it is positioned within the lipid membrane. There are two possible modes in which LfcinB could bind membranes. The first possibility is the formation of oligomeric pores. LfcinB would insert into the membrane so that its extended strands lie perpendicular to the membrane surface. Several LfcinB monomers would multimerize, so that the outer hydrophobic surface would interact with the membrane while the inner hydrophilic surface forms the inside of a transmembrane channel. This mechanism has been proposed for the defensins (*31*). In the alternative mode of membrane interaction, LfcinB interacts with a single leaflet of the lipid bilayer, so that its backbone lies parallel to the membrane surface. This mode of binding would be similar to that determined for the antimicrobial peptides magainin 2 (*50*), as determined by solid-state NMR, and cecropin P1 (*51*), as determined from attenuated total reflection FTIR. Based on its NMR solution structure, it is likely that LfcinB prefers the orientation parallel to the membrane bilayer.

It was found that a short hexapeptide fragment of LfcinB, RRWQWR-NH_2, retained antimicrobial activity (*9*). Similar antimicrobial hexapeptides have been identified: Ac-RRWWCO-NH_2, Ac-RRWWRO-NH_2, Ac-RRWCKO-NH_2, Ac-FRWLLO-NH_2, Ac-FRWWHO-NH_2, where "O" stands for an amino acid specific to each series (*52*). These hexapeptides emphasize the importance of Trp and Arg residues for antimicrobial activity, particularly in LfcinB. Trp has a partly hydrophobic and partly hydrophilic character (*53*), so that it prefers to partition at the hydrophobic−hydrophilic boundary of the membrane. In most membrane proteins, almost all Trp residues are found near the membrane surface (*54*, *55*). If LfcinB formed multimeric transmembrane pores, Trp6 and Trp8 would be placed unfavorably in the middle of the membrane bilayer. In addition, it is unlikely that the short lactoferricin fragment, RRWQWR-NH_2, forms a transmembrane structure. Rather, the hexapeptide might be expected to lie parallel to the membrane surface in an extended conformation, so that the Arg and Gln interact with the hydrophilic components, while the Trp residues are

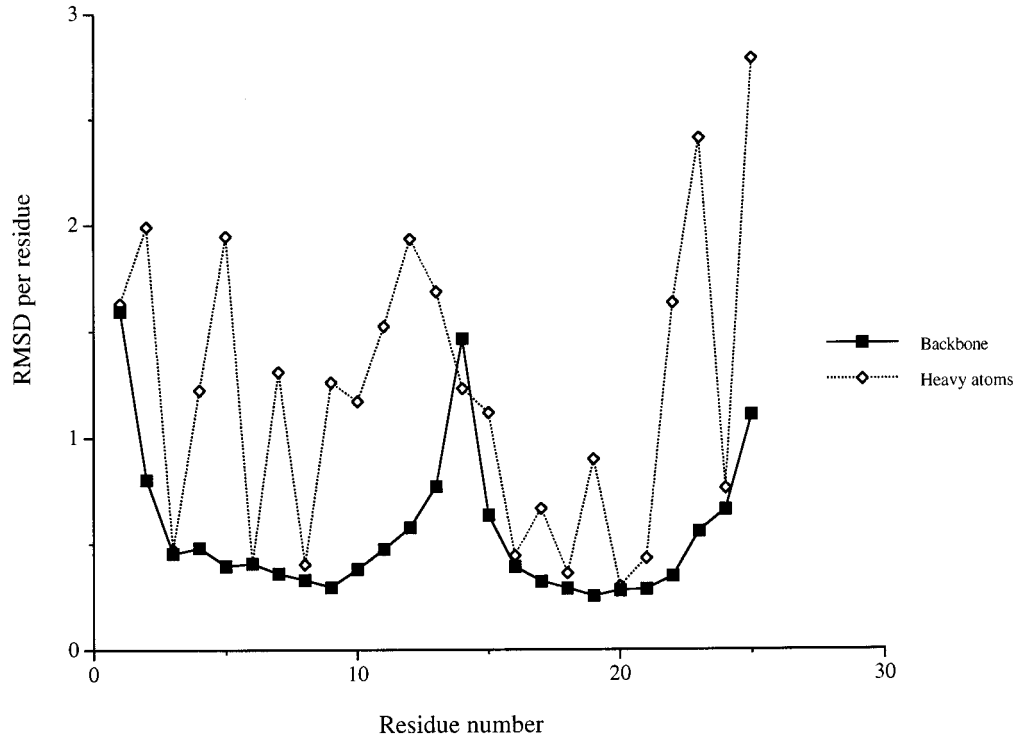

FIGURE 6: Plot of the root-mean-square deviation (RMSD) per residue for the 20 final structures of LfcinB. Heavy atoms include all atoms except hydrogen.

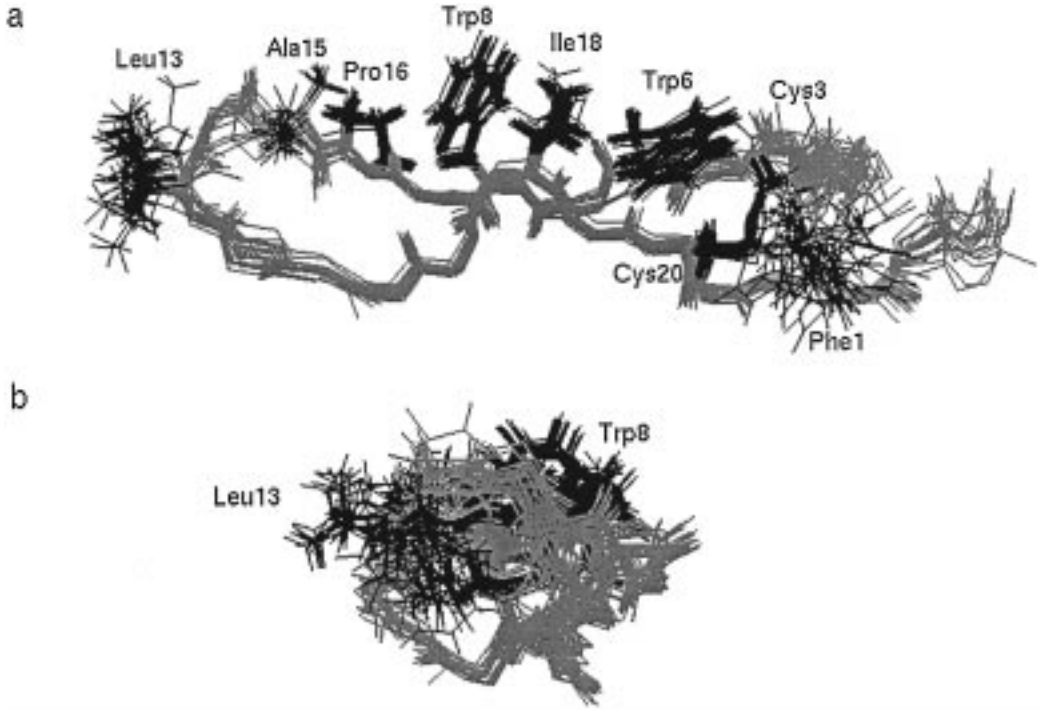

FIGURE 7: Hydrophobic core of LfcinB as seen from (a) across the β- strands and (b) along the β-strands, with the disulfide region pointed out of the page and the turn region pointed into the page and away from the observer. The backbone of all residues is shown in gray, while the highlighted side chains are black. The figure was generated using INSIGHTII.

placed at the membrane interface. Phe1, Cys3, Trp6, Trp8, Met10, Leu13, Ile18, Cys20, and Phe25 comprise all of the amino acids in LfcinB which could interact favorably with a membrane interface (*56*). If LfcinB were to lie parallel to the membrane, all of these residues could be placed on the same side of the β-sheet.

It is not certain how this form of peptide insertion would induce increased membrane permeability. LfcinB and other peptides may interact only with the outer leaflet, permeabilizing the membrane by interfering with lipid organization and packing. Yet, although the preferred orientation of the α-helical magainins and cecropins has been shown to be membrane-parallel, recent neutron scattering studies have shown that these peptides can indeed form transmembrane multimeric pores (*57*). The role of these multimeric pores and their relevance to the antimicrobial activity of magainins

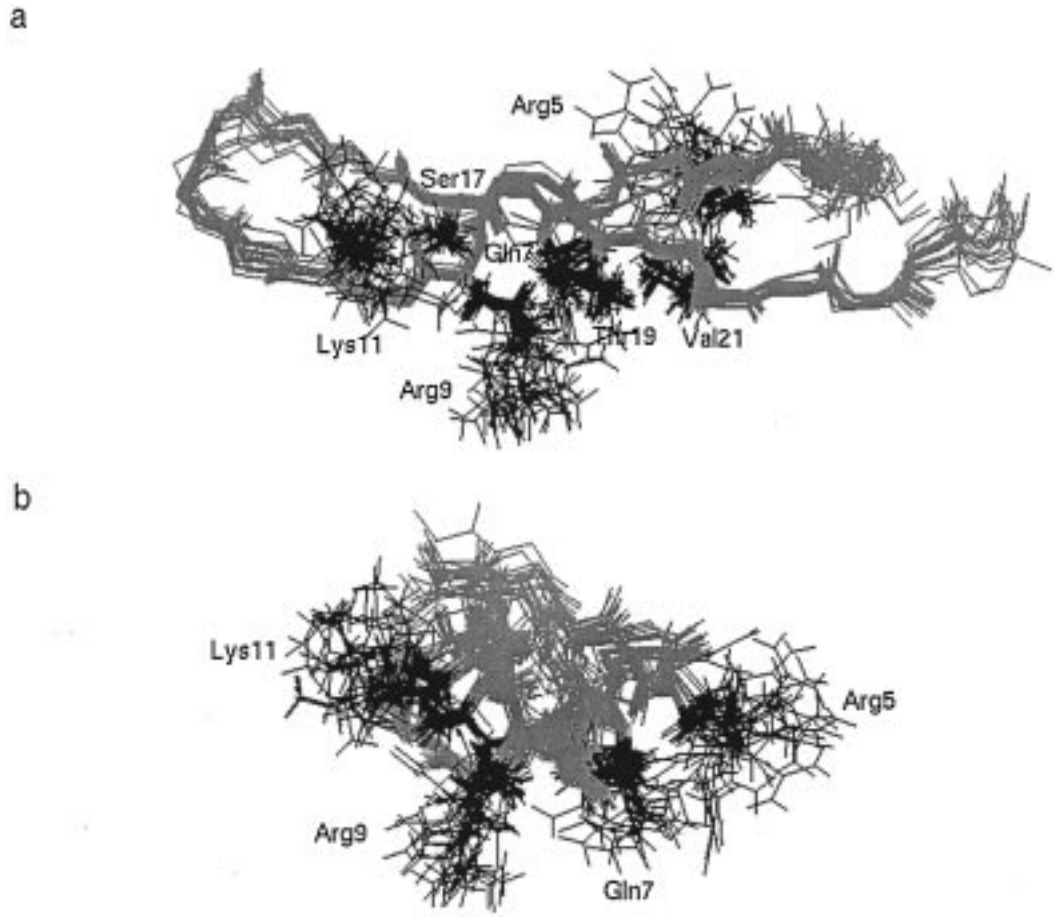

FIGURE 8: Hydrophilic side of LfcinB. Long-range NOE distance restraints were observed for all of the side chains shown. The orientations of 8a and 8b are identical to those in 7a and 7b. The backbone of all residues is shown in gray, while the highlighted side chains are black. The figure was generated using INSIGHTII.

and cecropins are still being intensively studied (*58*−*60*). It appears that pores are not formed at low concentrations of cecropins, even though antimicrobial activity can be detected (*58*).

Although the preferred orientation of intact LfcinB may be parallel to the membrane, it could possibly form a transmembrane multimeric pore. The extended β-sheet structure would certainly allow LfcinB to span a bilayer, and the many postive ends clustered near the disulfide bridge (Lys2, Arg4, Arg22, and Arg23) and near the turn (Lys11 and Lys12) may provide an electrostatic anchor on opposite sides of the bilayer. Still, as mentioned above, whether a transmembrane structure would be important to the actual antimicrobial mechanism is uncertain. One study suggested that the antimicrobial peptide tachyplesin I disrupted membranes by a pore-forming mechanism, but a linear analogue with protected Cys groups did so by interacting only with the outer leaflet (*61*). We note that the solution structure of tachyplesin resembles that of LfcinB, as it forms an amphiphilic β-sheet structure which is constrained by two disulfide bridges (*34*).

Comparison with the X-ray Structure of Bovine Lactoferrin. The NMR-derived secondary structure of LfcinB is markedly different from the X-ray structure of the same sequence in intact bovine lactoferrin (*37*). In the X-ray crystal structure, an alpha helix extends from Phe17 to Leu29 (Phe1 to Leu13 of LfcinB). Ser33 to Arg39 (Ser19 to Arg23) form an extended strand which participates in a parallel β-sheet with an N-terminal strand of bovine lactoferrin. The extended region from Ser17 to Arg23 is thus similar in both the X-ray and NMR structures. However, the long 13-residue helix (actually it extends N-terminally to include 5 more residues) in bovine lactoferrin is not present in the solution structure of lactoferricin B. Instead, an extended structure which forms one strand of a β-sheet is found.

Hydrophobic interactions may cause LfcinB to fold differently from intact bovine lactoferrin. In intact lactoferrin, Trp22 (Trp6 in LfcinB) and Met26 (Met10) are folded into the interior of domain 1, where they interact with Ala274, Phe278, Phe286, Leu288, and Leu299. These long-range hydrophobic interactions may encourage the formation of the α-helix in the intact protein, and these would not be present in the LfcinB peptide. This observation is in agreement with the notion that the secondary structure adopted by a sequence depends on the context in which it is found (*62*).

The β-sheet structure of LfcinB seems to be better suited for making initial contacts with membranes than the more helical structure found in intact lactoferrins. In the NMR-derived β-sheet structure, Trp6 and Trp8 adopt similar orientations, which would allow them to perform similar roles in interacting with the membrane interface. This contrasts the opposite orientations which the tryptophans adopt in a helical conformation. A recent circular dichroism study on

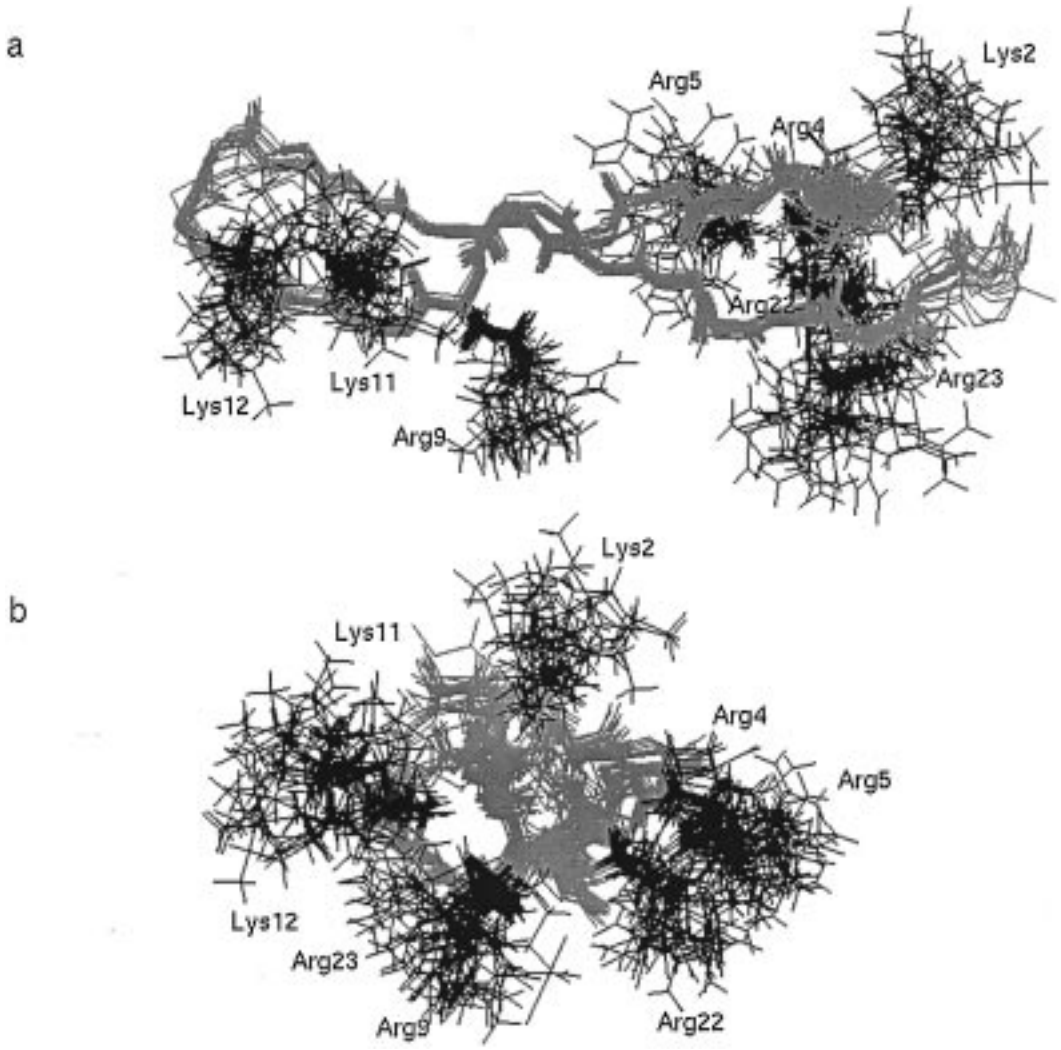

FIGURE 9: Postive side chains of LfcinB. The orientations of 9a and 9b are identical to those in 7a and 7b. The backbone of all residues is shown in gray, while the highlighted side chains are black. The figure was generated using INSIGHTII.

peptides related to LfcinB (*63*) found that when placed in trifluoroethanol (TFE), LfcinB was capable of forming an α-helix. However, when LfcinB was added to sodium dodecyl sulfate (SDS) micelles, significant helix formation was not detected, suggesting a different conformation. The latter result makes it unlikely—but does not exclude the possibility—that LfcinB can rearrange to a helical structure once it is inserted in a membrane. Further spectroscopic studies will have to address the structure of membrane-inserted LfcinB. Be that as it may, the amphiphilic β-sheet solution structure of LfcinB provides insight into the mechanism of membrane recognition by this antimicrobial peptide.

The $\alpha-\beta$ polymorphism observed here in LfcinB has also been detected for the prion protein responsible for Creutzfeldt–Jakob disease and the Aβ peptide, which has been implicated in Alzheimer's disease (*64*). In both cases, it is suspected that an α-to-β transition causes protein monomers to aggregate, leading to a pathological amyloid formation. The antimicrobial activity of lactoferrin may be an example of a beneficial α-to-β secondary structure transition. This transition can be induced by the release of LfcinB from bovine lactoferrin by pepsin cleavage. In the absence of this proteolytic activity, it is possible that membrane interactions alone are capable of inducing a similar α-to-β transition in the N-terminal region of intact lactoferrins.

ACKNOWLEDGMENT

We are indebted to Dr. D. McIntyre for his help in setting up NMR experiments; Dr. L. Kay for his 2D NOESY with WATERGATE pulse sequence; Dr. M. M. Moloney for use of the fluorescence spectrophotometer; and Dr. G. Lajoie for performing the mass spectrometry experiments. We appreciate the assistance of Ms. Margaret Tew with the typing of the manuscript.

REFERENCES

1. Masson, P. L., Heremans, J. F., and Dive, C. H. (1966) *Clin. Chim. Acta* 14, 735–739.
2. Masson, P. L., Heremans, J. F., and Schonne, E. (1969) *J. Exp. Med. 130*, 643–658.
3. Orseas, R., Yang, H., Baehner, R. L., and Boxer, L. A. (1981) *Blood 57*, 939–945.
4. Arnold, R. R., Cole, M. F., and McGhee, J. R. (1977) *Science* 197, 263–265.
5. Arnold, R. R., Brewer, M., and Gauthier, J. J. (1980) *Infect. Immun. 28*, 893–898.
6. Kirkpatrick, C. H., Green, I., Rich R. R., and Shade, A. L. (1971) *J. Infect. Dis. 124*, 539–544.

7. Soukka, T., Tenovuo, J., and Lenander-Lumikari, M. (1992) *FEMS Microbiol. Lett. 69*, 223−228.
8. Bellamy, W., Takase, M., Yamauchi, K., Wakabayashi, H., Kawase, K., and Tomita, M. (1992) *Biochim. Biophys. Acta 1121*, 130−136.
9. Tomita, M., Takase, M., Bellamy, W., and Shimamura, S. (1994) *Acta Paediatr. J. 36*, 585−591.
10. Wakabayashi, H., Hiratani, T., Uchida, K., and Yamaguchi, H. (1996) *J. Infect. Chemother. 1*, 185−189.
11. Yamauchi, K., Tomita, M., Giehl, T. J., and Ellison, R. T. (1993) *Infect. Immun. 61*, 719−728.
12. Appelmelk, B. J., An, Y.-Q., Geerts, M., Thijs, B. G., deBoer, H. A., MacLaren, D. M., deGraaf, J., and Nuijens, J. H. (1994) *Infect. Immun. 62*, 2628−2632.
13. Elass-Rochard, E., Rosanu, A., Legrand, D., Trif, M., Salmon, V., Motas, C., Montreuil, J., and Spik, G. (1995) *Biochem. J. 312*, 839−845.
14. Jones, E. M., Smart, A., Bloomberg, G., Burgess, L., and Millar, M. R. (1994) *J. Appl. Bacteriol. 77*, 208−214.
15. Brock, J. (1995) *Immunol. Today 16*, 417−419.
16. Crouch, P. M., Slater, K. J., and Fletcher, J. (1992) *Blood 80*, 235−240.
17. Mattsby-Baltzer, I., Roseanu, A., Motas, C., Elverfors, J., Engberg, I., and Hanson, L. A. (1996) *Pediatr. Res. 40*, 257−262.
18. Shau, H., Kim, A., and Golub, H. (1992) *J. Leukocyte Biol. 51*, 343−349.
19. Gahr, M., Speer, C. P., Damerau, B., and Sawatzki, G. (1991) *J. Leukocyte Biol. 49*, 427−433.
20. Bezault, J., Bhimani, R., Wiprovnick, J., and Furmanski, P. (1994) *Cancer Res.* 54, 2310−2312.
21. Yoo, Y.-C., Watanabe, H., Watanabe, R., Hata, K., Shimazaki, K., and Azuma, I. (1997) *Jpn. J. Cancer Res. 88*, 184−190.
22. Nicolas, P., and Mor, A. (1995) *Annu. Rev. Microbiol. 49*, 277−304.
23. Boman, H. G. (1995) *Annu. Rev. Immunol. 13*, 61−92.
24. Lee, J.-Y., Boman, A., Sun, C. X., Andersson, M., Jornvall, H., Mutt, V., and Boman, H. G. (1989) *Proc. Natl. Acad. Sci. U.S.A. 86*, 9159−9162.
25. Zasloff, M. (1987) *Proc. Natl. Acad. Sci. U.S.A. 84*, 5449−5453.
26. Holak, T. A., Engstrom, A., Kraulis, P. K., Lindeberg, G., Bennich, H., Jones, A., Gronenberg, A. M., and Clore, G. M. (1988) *Biochemistry 27*, 7620−7629.
27. Gesell, J., Zasloff, M., and Opella, S. (1997) *J. Biomol. NMR 9*, 127−135.
28. Odell, E. W., Sarra, R., Foxworthy, M., Chapple, D. S., and Evans, R. W. (1996) *FEBS Lett. 382*, 175−178.
29. Ganz, T., Selsted, M. E., Szklarek, Harwig, S. S. L., Daher, K., Bainton, D. F., and Lehrer, R. I. (1985) *J. Clin. Invest. 76*, 1427−1435.
30. Selsted, M. E., Tang, Y.-Q., Morris, W. K., McGuire, P. A., Novotny, M. J., Smith, W., Henschen, A. H., and Cullor, J. S. (1993) *J. Biol. Chem. 268*, 6641−6648.
31. Hill, C. P., Yee, J., Selsted, M. E., and Eisenberg, D. (1991) *Science 251*, 1481−1485.
32. Zimmerman, G. R., Legault, P., Selsted, M. E., and Pardi, A. (1995) *Biochemistry 34*, 13663−13671.
33. Fahrner, R. L., Dieckmann, T., Harwig, S. S. L., Lehrer, R. I., Eisenberg, D., and Feigon, J. (1996) *Chem. Biol. 3*, 543−550.
34. Kawano, K., Yoneya, T., Miyata, T., Yoshikawa, K., Tokunaga, F., Terada, Y., and Iwanaga, S. (1990) *J. Biol. Chem. 265*, 15365−15367.
35. Selsted, M. E., Novotny, M. J., Morris, W. L., Tang, Y.-Q., Smith, W., and Cullor, J. S. (1992) *J. Biol. Chem. 267*, 4292−4295.
36. Lawyer, C., Watabe, M., Borgia, P., Mashimo, T., Eagleton, L., and Watabe, K. (1996) *FEBS Lett. 390*, 95−98.
37. Moore, S. A., Anderson, B. F., Groom, C. R., Haridas, M., and Baker, E. N. (1997) *J. Mol. Biol. 274*, 222−236.
38. Anderson, B. F., Baker, H. M., Norris, G. E., Rice, D. W., and Baker, E. N. (1989) *J. Mol. Biol. 209*, 711−734.
39. Haridas, M., Anderson, B. F., and Baker, E. N. (1995) *Acta Crystallogr. D51*, 629−646.
40. Page, C. N., Vajdos, F., Fee, L., Grimsley, G., and Gray, T. (1995) *Protein Sci. 4*, 2411−2423.
41. Rance, M., Sorenson, O. W., Bodenhausen, G., Wagner, G., Ernst, R. R., and Wüthrich, K. (1983) *Biochem. Biophys. Res. Commun. 117*, 479−495.
42. Braunschweiller, L., and Ernst, R. R. (1983) *J. Magn. Reson. 53*, 521−528.
43. Jeener, J., Meier, B. H., Bachmann, P., and Ernst, R. R. (1979) *J. Chem. Phys. 71*, 4546−4553.
44. Sklenar, V., Piotto, M., Leppik, R., and Saudek, V. (1993) *J. Magn. Reson. Ser. A 102*, 241−245.
45. Delaglio, G., Grzesiek, S., Vuister, G. W., Zhu, G., Pfeifer, J., and Bax, A. (1995) *J. Biomol. NMR 6*, 277−293.
46. Johnson, B. A., and Blevins, R. A. (1994) *J. Biomol. NMR 4*, 603−614.
47. Wüthrich, K., Billeter, M., and Braun, W. (1983) *J. Mol. Biol. 169*, 949−961.
48. Brunger, A. T. (1992) *X-PLOR (Version 3.1) Manual*, Yale University Press, New Haven.
49. Wüthrich, K. (1986) *NMR of Proteins and Nucleic Acids*, John Wiley and Sons, New York.
50. Bechinger, B., Zasloff, M., and Opella, S. J. (1993) *Protein Sci. 2*, 2077−2084.
51. Gazit, E., Miller, I. R., Biggin, P. C., Sansom, M. S. P., and Shai, Y. (1996) *J. Mol. Biol. 258*, 860−870.
52. Blondelle, S. E., and Houghten, R. A. (1996) *Trends Biotechnol. 14*, 60−65.
53. Jacobs, R. E., and White, S. H. (1989) *Biochemistry 28*, 3421−3437.
54. Hu, W., Lee, K.-C., and Cross, T. A. (1993) *Biochemistry 32*, 7035−7047.
55. Reithmeier, R. A. F. (1995) *Curr. Opin. Struct. Biol. 5*, 491−500.
56. Wimley, W. C., and White, S. H. (1996) *Nat. Struct. Biol. 3*, 842−848.
57. He, K., Ludtke, S. J., and Huang, H. W. (1995) *Biochemistry 34*, 15614−15618.
58. Silvestro, L., Gupta, K., Weiser, J. N., and Axelsen, P. H. (1997) *Biochemistry 36*, 11452−11460.
59. Matsuzaki, K., Nakamura, A., Murase, O., Sugishita, K., Fujii, N., and Miyajima, K. (1997) *Biochemistry 36*, 2104−2111.
60. Matsuzaki, K., Murase, O., Fujii, N., and Miyajima, K. (1996) *Biochemistry 35*, 11361−11368.
61. Matsuzaki, K., Yoneyama, S., Fujii, N., Miyajima, K., Yamnada, K., Kirino, Y., and Anzai, K. (1997) *Biochemistry 36*, 9799−9806.
62. Minor, D. L., Jr., and Kim, P. S. (1996) *Nature 380*, 730−734.
63. Kang, J. H., Lee, M. K., Kim, K. L., and Hahm, K.-S. (1996) *Int. J. Pept. Protein Res. 48*, 357−363.
64. Mihara, H., and Takahashi, Y. (1997) *Curr. Opin. Struct. Biol. 7*, 501−508.

BI972323M